7 Tesla MRI with RF Power and Field Homogeneity Comparable to 4 Tesla using Computational Electromagnetics

L. Tang[2] and T. S. Ibrahim[1, 2]

[1.] Departments of Radiology and Bioengineering
University of Pittsburgh, Pittsburgh, Pennsylvania, USA
tsi2@pitt.edu (Correspondence)

[2]School of Electrical and Computer Engineering and Bioengineering Center
University of Oklahoma, Norman, Oklahoma, USA

Abstract – In ultrahigh (≥ 7 Tesla) field magnetic resonance imaging (MRI), the electromagnetic interactions between the coil, its excitation sources, and the biological load become more significant compared to low MRI applications. Computational electromagnetic (CEM) techniques are currently playing a major role in the evaluation of MRI radiofrequency (RF) coils (commonly now, within ultrahigh field context, referred to as transmit arrays).
This work compares the RF power requirements in 4 and 7 Tesla human MRI using CEM. Furthermore, we demonstrate that at ultrahigh MRI, high-quality/homogenous RF excitation fields could be obtained simultaneously with total RF power deposition lower than that achieved at lower field strengths. These results dispel what has been widely accepted from quasistatic approximations, namely that pushing the envelope of MRI field strength results in more RF power requirements and therefore, more RF power absorption in human tissue. This study is presented using the finite difference time domain (FDTD) method and a gradient-based optimization method.

Keywords: MRI, RF coil, transmit array, FDTD, optimization, RF power, B_1 field, coupling, and high filed.

I. INTRODUCTION

Since Magnetic Resonance Imaging (MRI) was first demonstrated in early 70s, MRI has become the primary technique in the routine diagnosis of many disease processes throughout the body. Although it faces some difficulties, operation at higher magnetic field strength and therefore higher frequency has been a constant goal for the advancement of MRI research. High field MRI brings the promise of high quality MR images as it is associated with increased signal-to-noise ratio [1], contrast-to-noise ratio, and high resolution. On the opposite end of the spectrum however, ultrahigh field (≥ 7 Tesla) imaging [2-4] is associated with significant technical complexities, the most notable of which is designing and building radiofrequency (RF) coils and/or transmit arrays. At such field strength, the complex interactions between the electromagnetic waves and the human head degrade the homogeneity of the MRI excitation field [5-6] (commonly referred to a B_1^+ field) and potentially increase the RF power absorption in the human head [7-8]. In order to analyze the electromagnetics of high frequency MRI, circuit/quasistatic approximations are no longer appropriate as the human head/body could be on the order of multiple wavelengths. As a result, full-wave CEM methods have been widely utilized for designing and predicting the performance of the RF coils/transmit arrays [6, 9, 10].

The interest in experimentally/theoretically investigating ultrahigh field technical and physical difficulties has been more academic than practical, since the technology to build ultrahigh field human systems did not exist. As field strength of human MRI magnets is growing at a staggering pace (currently performed at field strengths reaching 7 [3, 11], 8 [2, 12], and 9.4 [13] Tesla), accurately predicting and managing the RF power absorption and B_1^+ field homogeneity, associated with such operation has become essential to classify their future research potential as well as clinical practicality. A major hurdle that limits the clinical potential of ultrahigh field systems is finding means to improve the homogeneity of B_1^+ field distribution while maintaining acceptable RF power requirements to achieve it.

Unless combined with Transmit SENSE [14], for the purpose of improving the B_1^+ field homogeneity, it has been widely believed that the use of a phased array [15-16] (variable phase and variable amplitude) excitation with transmit arrays results in a significant increase in the total RF power deposition. In this paper, the FDTD method combined with a coupled-element coil model functioning as a transmitting phased array device were used to demonstrate that 7 Tesla human MRI can be

potentially achieved with 1) B_1^+ field distribution homogeneity, simultaneously with 2) total RF power deposition that are better than what is obtained at 4 Tesla using the same coupled-element coil operating under the standard quadrature excitation [17].

II. METHODS

A. The Coil Model

A 16-element transverse electromagnetic (TEM) resonator [12, 18] loaded with an anatomically detailed, 18-tissue, human head mesh [19] was utilized in this simulation study. The coil structure is composed of 16 elements, which are contained in an open cavity with the dimension of 34.6 cm in diameter and 21.2 cm in length. Each of the elements consists of coaxial line with a circular cross section. Two conductor rings are attached at the top and bottom of the cavity. The human head mesh is placed in the center of the coil such that the chin was aligned with the bottom ring. In our FDTD modeling approach, both the RF coil (including the coaxial rods, the shield, top and bottom rings, and excitation source(s)) and the human head mesh were modeled as a single system and therefore accounting for all of the coupling effects between the TEM resonator and the human head. The FDTD grid of the coil and human head mesh is shown in Fig. 1 (a). The in-house FDTD domain is divided into approximately 8 million cells with a resolution of 2 mm × 2 mm × 2mm. Perfectly matched layers (PML) [20] were used as the boundaries of the domain where 16 PML layers were placed on the 6 boundaries in the x, y, and z planes.

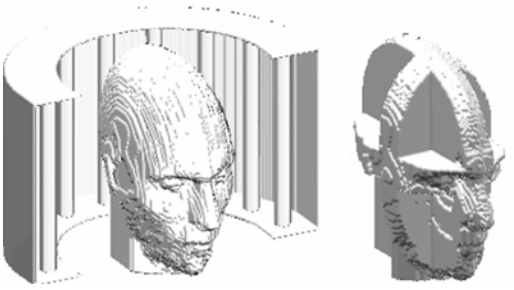

(a) (b)

Fig. 1. 3D FDTD model of the anatomically detailed human head mesh loaded within a 16-element TEM resonator (a) and the selected three 28mm slabs (b) oriented in axial, coronal and sagittal directions, respectively. In the simulations, the TEM resonator is completely surrounding the head model.

A stair-step approximation was used to model the coil shield and the top and bottom rings of the coil and a modified FDTD algorithm was used where the coaxial elements were modified into octagon shapes [19] to minimize the errors caused by stair stepping and to maintain an 8-fold symmetry.

B. Excitation and Tuning

The TEM resonator tuning was realized by adjusting the gap between each of the inner coaxial of elements with the load present in the coil. According to multi-conductor transmission line theory [21], there exist 9 modes exist in the 16-element TEM coil. The second mode (mode 1) on the spectrum is selected since at low frequencies/small electrical sizes, this mode produces a linearly polarized field in the center of the load. The resonating frequencies were set to 170 MHz (4 Tesla for ^{1}H imaging) and 295MHz (approximately 7 Tesla for ^{1}H imaging). The frequency spectra of the coil response are shown in Fig. 2.

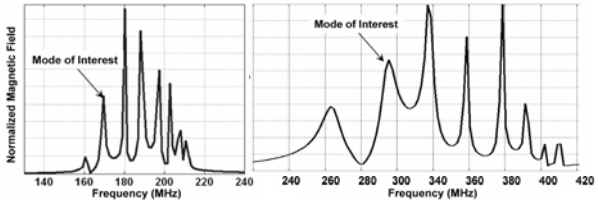

(a) (b)

Fig. 2. Frequency spectra for the 16-element TEM resonator loaded with the head model system at 4 Tesla (a) and 7 Tesla (b) by the FDTD method.

C. Experimental Validation

The aforementioned FDTD modeling technique has demonstrated excellent agreement with experimental measurements for this particular coil. Specifically this was achieved for predicting the 1) transmit and 2) receive magnetic fields and therefore 3) images as was shown in [6, 22], and 4) electric fields as was shown in [23] and therefore specific absorption rate and power deposition. To demonstrate the validity of multi-port excitation (the method utilized in this study), a similar highly-coupled TEM coil (8 elements) was modeled, built, and tested on a 7 Tesla human MRI system using 2-port excitation/reception. Arbitrarily chosen phase shifts (difference of 30 degrees between the coil excitation/reception ports) were implemented on the coil ports using costume made coaxial cables that are cut to these specifications. Figure 3 shows an excellent agreement between the FDTD calculations and the experimental images.

D. B_1^+ and Power Calculations

In MRI applications, the excitation magnetic field (typically referred to as B_1^+ field) is a circularly polarized component (in this study was chosen to possess clockwise rotational sense) of the total transverse, B_1, field as shown below,

$$B_1^+ = \left| \frac{B_{1x} + j * B_{1y}}{\sqrt{2}} \right|; \quad (1)$$

where B_{1x} and B_{1y} are the x and y components of the B_1 field, respectively. A homogenous B_1^+ field in a biological region of reset is needed in order to achieve useful MRI clinical information. In this study, a coefficient of variation (COV) is used to evaluate the homogeneity of B_1^+ field distribution. The total real input power entering the coil can be evaluated as,

$$P_{in} = P_{abs} + P_{rad} = \frac{\sigma}{2} \iiint_V \left| \vec{E} \right|^2 dv + \frac{1}{2} \iint_s (\vec{E} \times \vec{H}^*) \bullet d\vec{s} \quad (2)$$

where P_{abs} and P_{rad} are the absorbed and radiated power, respectively while $\iiint_v$ is the volume integral of the object to be imaged and $\iint_s$ is the integral of a closed surface that encloses the coil structure and the imaged object. The volume integration is done over the human head model. The surface integration is done by choosing a surface that encloses the coil and the sample and then performing the numerical integration over that surface.

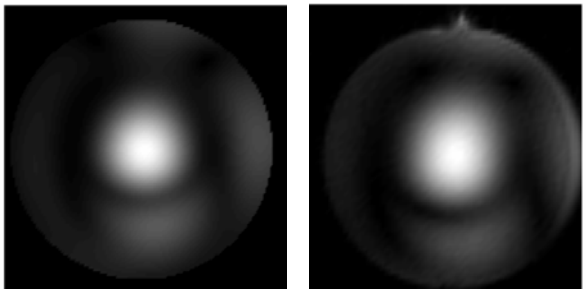

FDTD Simulations **7 tesla Experiment**

(a) (b)

Fig. 3. FDTD calculations (a) and experimental sagittal image (b) obtained using a 7 Tesla whole body system. The excitation/reception is performed in two ports using a TEM resonator loaded with 17-cm in diameter spherical phantom that posses dielectric constant = approx. 79 and conductivity = 0.46 S/m.

Because the percentage of the coil's radiated power (and therefore efficiencies) varies at different frequencies, the comparison of power requirements at different field strengths is unclear even for the same (geometry and dimensions) RF coil. More importantly, the absorbed power is associated with tissue dissipation and heating concerns. As a result, the absorbed power rather than the total power entering the coil was used in determining the power requirements in this study. In the FDTD domain, power absorbed was calculated from equation (3).

$$Power = \sum_i \sum_j \sum_k [\frac{1}{2} \sigma_{(i,j,k)} \times (E^2_{x_{(i,j,k)}} + E^2_{y_{(i,j,k)}} + E^2_{z_{(i,j,k)}})] \quad (3)$$

where $\sigma_{(i,j,k)}$ (S/m) is the conductivity of the FDTD cell at the (i,j,k) location; Ex, Ey and Ez (V/m) are the magnitudes of the electric field components in the x, y, and z directions, respectively; the summation is performed over the whole volume of the human head mesh.

E. Comparison Studies for the B_1^+ Distribution and Total Power Deposition

Using the FDTD mode, comparisons between 4 Tesla and 7 Tesla imaging were focused on homogeneity of the B_1^+ field and the power requirements to achieve the same excitation. By exciting all the elements of the coil in a phased-array fashion at 7 Tesla, variable phase/variable amplitude phased-array excitation was applied to achieve: 1) a coefficient of variation (COV) of the B_1^+ field in the region of interest with 2) total (in the whole human head mesh) RF power deposition lower than that obtained with 4-port fixed phases/amplitude (quadrature) excitation at 4 Tesla.

In the 4-port quadrature condition, all the 4 excitation sources were set with the same amplitude and $\pi/2$ phase shift between every two adjacent sources. 16-port optimized condition was carried-out by applying variable amplitude and phase for each excitation signal to achieve a better B_1^+ field distribution homogeneity within the region of interest and lower total power absorption. The optimization routine uses gradient algorithms were 32 unknown inputs (amplitude and phase variables) are varied to lower 1) the COV of B_1^+ field over slices and slabs with various orientations as well as 2) total power absorption by the human head mesh. In our calculation, B_1^+ field was normalized to 1.174μT, which is the field strength needed to produce a flip angle of $\pi/2$ with a 5-msec rectangular RF pulse; the power requirement is the scale to obtain the same B_1^+ field intensity.

III. RESULTS AND DISCUSSION

Optimization of the B_1^+ field was done on the slices (2mm thickness) and slabs (28mm thickness) oriented in the axial, coronal, and sagittal directions (as shown in Fig. 1 (b)) at 7 tesla in order to obtain more homogeneous B_1^+ field distribution (target is the 4Tesla/4port quadrature excitation COV) and lower total RF power absorption by the whole head mesh (target is the 4Tesla/4port quadrature excitation total power absorption for a fixed average B_1^+ field intensity in the region of interest). Similar to fluid-dynamics Mach number [24], the optimization target combines these two parameters into a non-linear relationship and was constantly changing throughout the iterations.

A. B_1^+ Field Distributions and Total RF Power Absorption

Figure 4 and Table 1 show the results including the B_1^+ field distributions and the associated RF power

deposition using 4-port quadrature excitation at 4 and 7 Tesla and 16-port variable phases/amplitude excitation for 2mm/28mm axial, coronal and sagittal slabs.

Table 1. The coefficient of variations and the total RF power absorption for the B_1^+ field distributions shown in Fig. 4.

Excite Condition	1-- 4T/4P Qua		2-- 7T/4P Qua		3-- 7T/16Pt Opt	
Parameter	COV	Power (w)	COV	Power (w)	COV	Power (w)
A (Axial Slice)	0.18	0.89	0.30	2.22	0.18	0.80
C (Coronal Slice)	0.25	1.17	0.30	2.44	0.24	0.99
S (Sagittal Slice)	0.24	1.09	0.25	2.16	0.23	1.04
A_Slab (Axial_slab)	0.18	0.92	0.31	2.44	0.18	0.77
C_Slab (Coronal_slab)	0.24	1.18	0.30	2.62	0.24	0.91
S_Slab (Sagittial_slab)	0.24	1.10	0.25	2.22	0.24	1.01

The results from a 4-port quadrature excitation at 4 and 7 Tesla demonstrate that the increased electromagnetic wave interactions in high field strength (7 Tesla) cause a decrease of B_1^+ field uniformity under the same excitation conditions. Additionally, the power required to obtain the same average B_1^+ field intensity (over a slice/slab of interest) increases at 7 Tesla compared to 4 Tesla. When a 16-port variable phases/amplitude excitation is applied however, the B_1^+ field uniformity can be greatly improved while significantly reducing the total absorbed power. From the data shown in Table 1, under 7 Tesla/16 port optimized conditions, 1) the B_1^+ field homogeneity over 2D slices and 3D slabs were improved to the same level of the ones under 4Tesla/4port quadrature conditions, with 2) the associated total RF power absorptions at 7 Tesla lower than that at 4 Tesla.

B. Distributions of the RF Power Absorbed in Tissue

To compare the effects of homogenizing the B_1^+ field homogeneity on RF power absorption, the distributions of the power deposition inside the head model were calculated and are displayed under different excitation conditions in Fig. 5. Coefficient of variations (COV) of the RF power distributions (corresponding to each subfigure in Fig. 5) are given in Table 2. This set of results show that, with similar total absorbed power, the power deposition (and therefore potential temperature rises) inside the head mesh varies under quadrature and optimized excitation conditions. Compared to quadrature excitation, the power absorption by tissue is more uniformly distributed with optimized excitation. Spreading the energy deposition through the whole head reduces the probability of local spots.

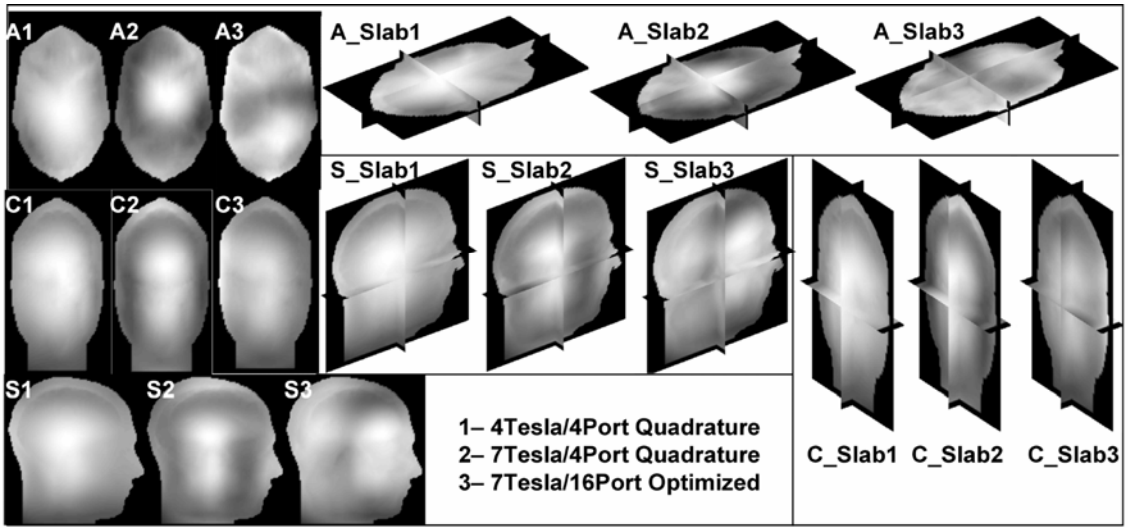

Fig. 4. The B_1^+ field distributions over axial (A1-A3), coronal (C1-C3) and sagittal (S1-S3) slices as well as axial (A_Slab1-3), coronal (C_Slab1-3) and sagittal (S_Slab1-3) slabs at 4 Tesla and 7 Tesla under different excitation conditions. 1, 2, and 3 represent the different excitation types as annotated in the figure.

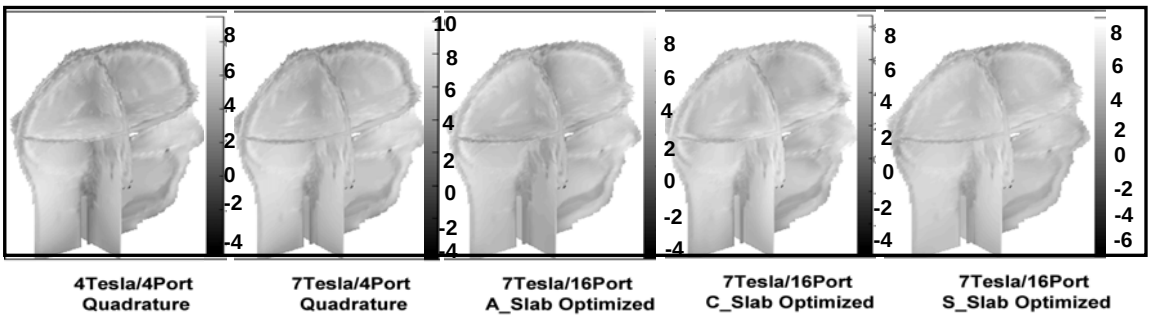

Fig. 5. Power distributions (dB) over the whole head mesh under different excitation conditions.

Table 2. The coefficient of variations for the RF power distributions (over the whole head mesh) shown in Fig. 5.

Excit-ation Types	4T/4P Qua.	7T/4P Qua.	7T/16P A_Slab Opt.	7T/16P C_Slab Opt.	7T/16P S_Slab Opt.
COV	0.56	0.50	0.45	0.41	0.40

As such with the optimization scheme presented in this work, compared to 4 Tesla 4-port quadrature excitation, more homogeneous B_1^+ field (as denoted by lower COV) simultaneously with lower total RF power absorption could be obtained at 7 Tesla. The presented results dispel what has been widely accepted from quasistatic approximations namely that pushing the envelope of MRI field strength results in more RF power requirements and therefore more RF power absorption in human tissue. The numerical simulations presented in this work indicate that the severe inhomogeneity associated with quadrature excitation at 7 Tesla is resultant from the lack of a B_1^+ field but not necessarily from the lack of electromagnetic energy. The rearrangement of B_1^+ field distribution or increase of B_1^+ field intensity affects only a component of the total RF magnetic field and does not necessarily cause increases in total RF power absorption.

IV. CONCLUSION

In high and ultra high field human MRI applications, computational electromagnetic techniques are playing a significant role in the design of the needed RF coils/transmit arrays and excitation approaches to obtain high quality images and manage the RF power deposition. Utilizing FDTD method, this work demonstrates that homogenous excitation can be achieved at 7 Tesla MRI for human head applications with a lower than the amount of RF power required for 4 Tesla MRI.

ACKNOWLEDGEMENT

The authors would like to acknowledge YiK-Kiong Hue for his assistance in creating the numerical result in Fig. 3.

REFERENCES

[1] D. I. Hoult and R. E. Richards, "The signal-to-noise ratio of the nuclear magnetic resonance experiment," *Journal of Magn. Reson. (1969)*, vol. 24, pp. 71-85, 1976.

[2] P. M. L. Robitaille, A. M. Abduljalil, A. Kangarlu, X. Zhang, Y. Yu, R. Burgess, S. Bair, P. Noa, L. Yang, H. Zhu, B. Palmer, Z. Jiang, D. M. Chakeres, and D. Spigos, "Human magnetic resonance imaging at 8 T," *Nmr in Biomedicine*, vol. 11, pp. 263-265, 1998.

[3] J. T. Vaughan, M. Garwood, C. M. Collins, W. Liu, L. DelaBarre, G. Adriany, P. Andersen, H. Merkle, R. Goebel, M. B. Smith, and K. Ugurbil, "7T vs. 4T: RF power, homogeneity, and signal-to-noise comparison in head images," *Magn. Reson. Med.*, vol. 46, pp. 24-30, 2001.

[4] B. Beck, D. H. Plant, S. C. Grant, P. E. Thelwall, X. Silver, T. H. Mareci, H. Benveniste, M. Smith, C. Collins, S. Crozier, and S. J. Blackband, "Progress in high field MRI at the University of Florida," *Magma*, vol. 13, pp. 152-7, 2002.

[5] T. S. Ibrahim, R. Lee, A. M. Abduljalil, B. A. Baertlein, and P. M. Robitaille, "Dielectric resonances and B(1) field inhomogeneity in UHFMRI: computational analysis and experimental findings," *Magn. Reson. Imaging*, vol. 19, pp. 219-26, 2001.

[6] T. S. Ibrahim, C. Mitchell, P. Schmalbrock, R. Lee, and D. W. Chakeres, "Electromagnetic perspective on the operation of RF coils at 1.5-11.7 Tesla," *Magn. Reson. Med.*, vol. 54, pp. 683-90, 2005.

[7] C. M. Collins and M. B. Smith, "Signal-to-noise ratio and absorbed power as functions of main magnetic field strength, and definition of "90 degrees" RF pulse for the head in the birdcage coil," *Magn. Reson. Med.*, vol. 45, pp. 684-91, 2001.

[8] D. I. Hoult, C. N. Chen, and V. J. Sank, "The field dependence of NMR imaging. II. Arguments concerning an optimal field strength," *Magn. Reson. Med.*, vol. 3, pp. 730-46, 1986.

[9] O. P. Gandhi and X. Bin Chen, "Specific absorption rates and induced current densities for an anatomy-based model of the human for exposure to time-varying magnetic fields of MRI," *Magn. Reson. Med.*, vol. 41, pp. 816-823, 1999.
[10] J. Chen, Z. M. Feng, and J. M. Jin, "Numerical simulation of SAR and B-1-field inhomogeneity of shielded RF coils loaded with the human head," *IEEE Transactions on Biomedical Engineering*, vol. 45, pp. 650-659, 1998.
[11] L. L. Wald, G. C. Wiggins, A. Potthast, C. J. Wiggins, and C. Triantafyllou, "Design considerations and coil comparisons for 7 T brain imaging," *Applied Magn. Reson.*, vol. 29, pp. 19-37, 2005.
[12] T. S. Ibrahim, A. Kangarlu, and D. W. Chakeress, "Design and performance issues of RF coils utilized in ultra high field MRI: experimental and numerical evaluations," *IEEE Transactions on Biomedical Engineering*, vol. 52, pp. 1278-84, 2005.
[13] J. T. Vaughan, "How to do RF at high fields," in *The International Society of Magn. Reson. Med. Annual Meeting: MORNING CATEGORICAL COURSE: Human MRI and MRS at High Static Magnetic Fields*. Miami, Florida: ISMRM, 2005.
[14] U. Katscher, J. Rohrs, and P. Bornert, "Basic considerations on the impact of the coil array on the performance of Transmit SENSE," *Magn. Reson. Materials in Physics Biology and Med.*, vol. 18, pp. 81-88, 2005.
[15] T. S. Ibrahim, R. Lee, B. A. Baertlein, A. Kangarlu, and P. L. Robitaille, "Application of finite difference time domain method for the design of birdcage RF head coils using multi-port excitations," *Magn. Reson. Imaging*, vol. 18, pp. 733-42, 2000.
[16] F. Liu, B. L. Beck, J. R. Fitzsimmons, S. J. Blackband, and S. Crozier, "A theoretical comparison of two optimization methods for radiofrequency drive schemes in high frequency MRI resonators," *Physics in Med. and Biology*, vol. 50, pp. 5281-5291, 2005.
[17] G. H. Glover, C. E. Hayes, N. J. Pelc, W. A. Edelstein, O. M. Mueller, H. R. Hart, C. J. Hardy, M. O'Donnell, and W. D. Barber, "Comparison of linear and circular polarization for magnetic resonance imaging," *Journal of Magn. Reson. (1969)*, vol. 64, pp. 255-270, 1985.
[18] J. T. Vaughan, H. P. Hetherington, J. O. Otu, J. W. Pan, and G. M. Pohost, "High-frequency volume coils for clinical NMR imaging and spectroscopy," *Magn. Reson. Med.*, vol. 32, pp. 206-218, 1994.
[19] T. S. Ibrahim, "Ultrahigh-field MRI whole-slice and localized RF field excitations using the same RF transmit array," *IEEE Transactions on Medical Imaging*, vol. 25, pp. 1341-7, 2006.
[20] J. P. Berenger, "A perfectly matched layer for the absorption of electromagnetic-waves," *Journal of Computational Physics*, vol. 114, pp. 185-200, 1994.
[21] B. A. Baertlein, O. Ozbay, T. Ibrahim, R. Lee, Y. Yu, A. Kangarlu, and P. M. Robitaille, "Theoretical model for an MRI radio frequency resonator," *IEEE Transactions on Biomedical Engineering*, vol. 47, pp. 535-46, 2000.
[22] T. S. Ibrahim, C. Mitchell, R. Abraham, and P. Schmalbrock, "In-depth study of the electromagnetics of ultrahigh-field MRI," *NMR Biomed*, vol. 20, pp. 58-68, 2007.
[23] T. S. Ibrahim and R. Lee, "Evaluation of MRI RF probes utilizing infrared sensors," *IEEE Transactions on Biomedical Engineering*, vol. 53, pp. 963-967, 2006.
[24] J. H. Zhao, J. O. Burns, M. L. Norman, and M. E. Sulkanen, "Instabilities in astrophysical jets .2. numerical simulations of slab jets," *Astrophysical Journal*, vol. 387, pp. 83, 1992.

Lin Tang received her B.S. degree in physics from Sichuan University, China, in 1999 and M.S. degree in physics from University of Oklahoma, US, in 2005. She is currently a Ph.D. candidate of electric and computer engineering at University of Oklahoma. Her research interests include performance of high field magnetic resonance imaging (MRI) and computational electromagnetics.

Tamer S. Ibrahim received his B.S. with distinction and honors in electrical engineering and with option in computer science, M.S.E.E, and Ph.D. degrees from Ohio State University in 6/96, 12/98, and 3/03, respectively. Since 01/03, he has been an assistant professor in The School of Electrical and Computer Engineering and a Faculty Member in The Bioengineering Center at University of Oklahoma; since 02/06 he has been an assistant professor in the Departments of Radiology and Bioengineering at the University of Pittsburgh. Dr. Ibrahim is the technical director for human ultra high field magnetic resonance imaging (MRI) at the University of Pittsburgh where he leads the radio-frequency research and development for human and animal MRI. His research also focuses on the development of wireless micro-neural interfaces, radome characterization technology, and wireless sensor networks for intelligent high-way systems. Dr. Ibrahim has authored/co-authored more than 115 scientific journal articles/book chapters/international conference proceedings; since 01/06, his average ISI, non-self, citations has ranged between 4-5 times per month. He has given numerous plenary/educational seminars in International meetings and research centers. He was the recipient of the ElectroScience Laboratory's Outstanding Journal Paper and Master Thesis Awards and of conference paper awards at IEEE Antenna and Propagation Society and International Society of Magnetic Resonance in Medicine Meetings. His biography is listed in *Who is Who* of *Emerging Leaders*, *American Education*, *Science and Engineering*, and *America*. Dr. Ibrahim has served as a reviewer for numerous journals and for funding agencies such as NIH, NSF, and DOD. Currently, he serves as an Associate Editor of the International Journal on Antennas and Propagation and as a member of the NIH Small Business Medical Imaging Technology Study Section.